

Automatic Lung Nodule Detection Using Profile Matching and Back-Propagation Neural Network Techniques

Shih-Chung B. Lo, Matthew T. Freedman, Jyh-Shyan Lin, and Seong K. Mun

The potential advantages of using digital techniques instead of film-based radiography have been discussed extensively for the past 10 years. A major future application of digital techniques is computer-assisted diagnosis: the use of computer techniques to assist the radiologist in the diagnostic process. One aspect of this assistance is computer-assisted detection. The detection of small lung nodule has been recognized as a clinically difficult task for many years. Most of the literature has indicated that the rate for finding lung nodules (size range from 3 mm to 15 mm) is only approximately 65%, in those cases in which the undetected nodules could be found retrospectively. In recent published research, image processing techniques, such as thresholding and morphological analysis, have been used to enhance true-positive detection. However, these methods still produce many false-positive detections. We have been investigating the use of neural networks to distinguish true-positives nodule detections among those areas of interest that are generated from a signal enhanced image. The initial results show that the trained neural networks program can increase true-positive detections and moderately reduce the number of false-positive detections. The program reported here can perform three modes of lung nodule detection: thresholding, profile matching analysis, and neural network. This program is fully automatic and has been implemented in a DEC 5000/200 (Digital Equipment Corp, Maynard, MA) workstation. The total processing time for all three methods is less than 35 seconds. In this report, key image processing techniques and neural network for the lung nodule detection are described and the results of this initial study are reported.

Copyright © 1993 by W.B. Saunders Company

KEY WORDS: Lung nodule detection, computer-assisted diagnosis, neural network, and digital imaging.

IN DIGITAL MEDICAL imaging, research and development in computerized imaging modalities (eg, computed tomography, computed radiography, and magnetic resonance

imaging, etc) have been growing very rapidly. The development of picture archiving and communications systems (PACS) has been greeted with great enthusiasm.¹⁻³ Besides rapid digital communication and huge on-line storage using the current digital technology for medical imaging, clinicians are also interested in potential applications of artificial intelligence in medicine based on advanced computer power. Medical imaging, artificial intelligence, and computer technology are closely associated and have common goals in the improvement of patient care. These research activities are currently being pursued in the radiology research community.

Although skilled pulmonary radiologists have a high degree of accuracy in diagnosis, problems remain in the detection of disease, problems that cannot be corrected with current methods of training and high levels of clinical skill and experience. These problems include the miss rate for detection of small pulmonary nodules, the detection of minimal interstitial lung disease, and the detection of changes in pre-existing interstitial lung disease. Enhancing the detection of small pulmonary nodules by computer-assisted diagnosis, the goal of this project, is important because studies in the use of chest radiographs for the detection of lung nodules^{4,5} have shown that even with highly skilled and highly motivated radiologists who are task-directed to detect any finding suspicious for a pulmonary nodule and working with high quality chest radiographs, only 68% of all retrospectively detected lung cancers were detected prospectively when read by one reader, and only 82% were detected by two readers. In the series reported by Stitik, many of the missed lesions would be classified as $T_1M_xN_x$ lesions, the stage of non-small cell lung cancer that Mountain indicates has the best prognosis (42%, 5-year survival).⁶ This is the same stage of lung cancer that our current computer-assisted diagnostic program has proven best in detecting (nodules 3 to 20 mm in diameter, separate from the hilum). In Stitik's analyses, the three most frequent causes of error are: observer error, ill defined lesions, and lesions overlying bone.

From the Radiology Department, Georgetown University Medical Center, Washington, DC.

Supported in part by AGFA-Gevaert Corp (Mortsel, Belgium) and a computer system support made by Digital Equipment Corp (Maynard, MA).

Address reprint requests to Shih-Chung B Lo, PhD, Radiology Department, Georgetown University Medical Center, 3800 Reservoir Road NW, Washington, DC 20007.

*Copyright © 1993 by W.B. Saunders Company
0897-1889/93/0601-0007\$05.00/0*

The current film/screen procedure and current radiologist reading techniques have been practised for many years, and the diagnostic yield from the established techniques is not likely to improve. Alternative methods are therefore of potentially great clinical importance. Because cost-effective high speed computers, such as the "reduced instruction set"-type computers, which can range from 25 to 75 million instructions per second, are applied to the rapidly developing areas of pattern recognition and artificial intelligence, the use of these techniques for radiographic pattern recognition becomes a practical and quick method to assist the radiologist by serving as an additional check on the radiologists skills at disease detection.

MATERIAL AND METHODS

Chest radiographs for patients who have primary and metastatic cancer and one or several lung nodules are converted into digital form using a laser film digitizer. The digital data are transmitted and stored in our PACS until needed for the research project. The images are then retrieved to a high speed workstation. Sequential computer searches are then performed consisting of a thresholding evaluation, use of background subtraction for nodule enhancement, a test of profile matching rate, and, finally, neural network classification. It takes 25 to 35 seconds to search for suspected nodules and report the probability (ie, confidence level) of having a nodule in the area.

Clinical Cases

We selected 30 patients who had primary or metastatic cancer (and, in some cases, one or several who had calcified granulomata) whose chest radiographs each contained one or several lung nodules of 3 to 15 mm in size, separated from the hilum. We selected 3 mm as the minimum size because most radiographically detectable nodules are larger than 3 mm in diameter (ie, ≈ 18 pixels in $2,048 \times 2,500$). We selected additional patients as normal controls from patients without known cancer and with chest radiographs considered by two radiologists to be free of nodules.

Film Digitization Method

The selected chest radiographic images are converted to digital format with a laser film digitizer (Konica Laser Film Scanner Model: KDFR-S; Tokyo, Japan). This scanner undergoes routine quality control test including⁷ gray value response, spatial linearity, flat field uniformity, and frequency response function (or modulation transfer function).

Once digitized, the image data is transmitted to a Micro-VAX II computer (the host of the film scanner) through a DR11-W channel. These images are formatted in $2,048 \times 2,500 \times 10$ bits of computer information (for a 14 inch \times 17 inch area where each image pixel represents $175 \mu\text{m}$ square). These images can be sent to the PACS and/or the high speed workstation. Each pulmonary radiograph is shrunk to $512 \times 625 \times 12$ bits by a convolution process.⁸ This reduces the number of calculations by a factor of 16.

Imaging Processing for Enhancement of Lung Nodule Detectability

Potential nodule information in a pulmonary radiograph was enhanced by subtracting a nodule suppressed image (ie, a kernel size of 15 mm for the median filter) from a nodule enhanced image (ie, a matched filter of a sphere profile with 15 mm in diameter). Besides median and match filters, the nodule enhanced algorithms involve two-dimensional fast Fourier transfer and background correction. The algorithms were composed as indicated in Fig 1.⁹ We call the resulting image a "nodule enhanced image."

Suspected Lung Nodule Extraction and Determination

Feature extraction to detect round or nearly round objects is conducted on the nodule enhanced image as the first step in the nodule searching procedure. This image is processed by a feature extraction technique using edge and gray value tracking with different gray values for thresholding.^{9,10} This is followed by a sphere profile matching techniques involving two steps:

Feature extraction. Once an area meets criteria for a possible nodule based on edge detection and gray value thresholding, the image block of the area (32×32 pixels representing $55 \text{ mm} \times 55 \text{ mm}$ on the original image) is selected for further analysis. First the image block is background corrected and processed for background removal. The latter is done by calculating the averaged value

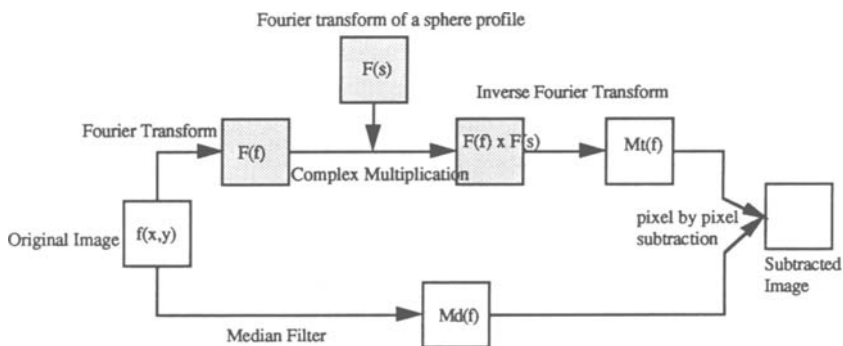


Fig 1. Processes of the nodule enhancement.

of the pixels just outside the tracking boundaries on the background corrected image. These tracking boundaries are the corresponding boundaries of the initial area search on the nodule enhanced image.

Sphere profile matching technique. A sphere profile matching technique is then used. Several two-dimensional synthetic sphere profiles corresponding to various diameters were made and stored in the computer memory or disk. Each profile has a third dimension representing normalized intensity. The density in the profile area is proportional to the integration of attenuation through a sphere.

After the suspected area has its background removed, the area equivalent synthetic profile is fetched for the calculation of the matching rate given below:

$$M_r = \frac{\sum A(x, y)S(x, y)}{[\sum A^2(x, y)]^{1/2}[\sum S^2(x, y)]^{1/2}} \quad (1)$$

where $S(x, y)$ is the synthetic nodule block and $A(x, y)$ is the background subtracted image block which is given by:

$$A(x, y) = f'(x, y) - B \quad (2)$$

where $f'(x, y)$ denotes the background corrected image block and B is the calculated background value.

To obtain the reasonable matching rate, several constants, one constant at a time, are added to (or subtracted) from the background eliminated image block (B). These calculations are used to search for the greatest match with a profile—we used a maximum matching rate in this experiment. The higher the values of the matching rates obtained in the corresponding extracted image block, the higher the probability that a nodule is in the area. We preset three different levels of matching rate for various detection sensitivities: low confidence (high sensitivity)—0.8 to 0.85, moderate confidence (moderate sensitivity)—0.85 to 0.9, and high confidence (low sensitivity)—0.9 to 1.0. A brief set of computer execution steps is given below:

- Step 0: Search a pixel value greater than the threshold value.
- Step 1: Trace the boundary of an area containing pixel values greater than the threshold value.
- Step 2: Find the centroid of the area.
- Step 3: Artificially make (or retrieve from memory) a two-dimensional sphere profile having an equivalent radius.
- Step 4: Calculate the matching rate between the artificial profile and the suspected area.
- Step 5: Find the most probable case of matching.
- Step 6: Mask the area with a value below the threshold value (eg, 0).
- Step 7: Go back Step 0 to continue.

Through the nodule enhancing processes and matching rate determination, all round and nearly round objects in the nodule-enhanced image are selected. However, many vessel spots, vessel clusters, and some rib crossing areas are also sometimes identified as suspected areas (ie, at this point the sensitivity of the system is 100%, but the specificity is low). These are false-positive detections and an additional step (the neural network) is used to decrease their frequency.

Nodule Detection Using a Back-Propagation Neural Network

A neural network has been trained as a classifier to help to distinguish the rib crossings and round vessels from the true nodules. The results of our initial attempt are encouraging and are reported below.

Clinical cases used. Image blocks used for both the training and testing of the neural network were selected from true-positive and false-positive detections based on the nodule detection computer program running in the high sensitivity selection mode (ie, matching rate > 0.7). For training the neural network, the database was divided into three categories: non-nodule, nodule, and calcified nodule cases. All classifications were confirmed by the radiologist.

Training cases. The neural network was trained on extracted 32 pixel \times 32 pixel boxes taken from chest images. The true nodule cases were taken from chest images of patients who had cancer metastatic to the lung, each of which contained several lung nodules. In experiments 1 and 2 (described below) the normal training images were obtained from chest images in patients without known cancer considered by at least two radiologists to be free from nodules. For both experiments, original images including their extracted image blocks are separated into two categories: for training and testing. For experiment 3, 30% of nodule-free image blocks for training come from test images in which each image contains a single true nodule. However, no image blocks are reused for both training and testing.

Nodules considered to be calcified included nodules unequivocally calcified and those thought to be calcified and unchanged for at least 1 year.

Test cases. The lung nodule cases used to test the neural network were mainly those in which the patients had a single proved nodule. Three cases with several metastatic nodules were also included in the true-positive category, each contributing one nodule to the series.

The Neural Network Structure and Back-Propagation: Training the Neural Network

The structure of the neural network. The neural network¹¹ was established by a two-layer structure (ie, single hidden layer neural network): (1) the input layer which consists of 1,024 nodes and each node accepts each pixel value on the image block (32 \times 32 elements); (2) the hidden layer which consists of 100 to 200 nodes in this experiment; and (3) the output layer which has two or three nodes. The nodes between adjacent layer are fully connected. Figure 2 shows the construction of this neural network.

On the output layer, node 0, is assigned to non-nodule cases, node 1 is assigned to nodule cases, and node 2 is

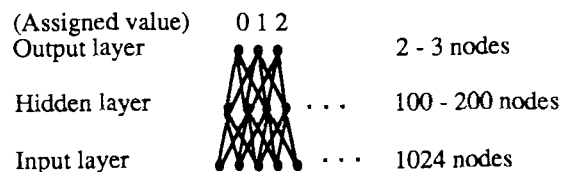


Fig 2. A neural network structure for evaluation of lung nodule blocks.

RESULTS

Convergence of The Neural Network

Using this network with its preset factors, the sum of the square output errors converged starting from approximately 200 iterations and continuing up to 400 to 500 iterations for all training. Image blocks in the training set receive 100% correct detection of nodule and non-nodule when the cutoff is set at 0.5 for the normalized output value at node 1 (or the sum of nodes 1 and 2). The results including the receiver operating characteristic (ROC) curve of the performance response are illustrated in the following section.

Classification Accuracy of The Neural Network

Experiment 1. The training set was four images consisting of 20 multiple nodules and 40 false nodules detected from the preliminary evaluation. The test set was 26 images consisting of 39 true nodules and 135 false nodules. The number of nodes on the hidden layer was 200, and the number of output nodes was 3.

Figure 4 shows an ROC curve in which $A(z)$ is 0.634 with standard deviation (SD) 0.049 (where $A(z)$ denotes the area under the curve).

Experiment 2. The training set was four images consisting of 20 multiple nodules and 40 false nodules detected from the preliminary evaluation. The test set was 26 images consisting of 39 true nodules and 135 false nodules. The number of nodes on the hidden layer was 100, and the number of output nodes was two.

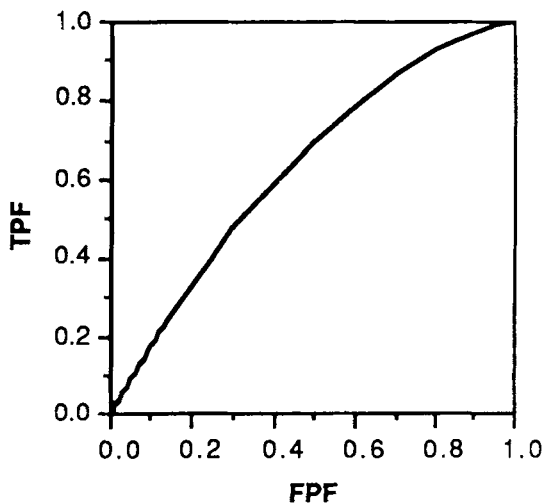


Fig 4. An ROC curve in which $A(z)$ is 0.634 with SD = 0.049.

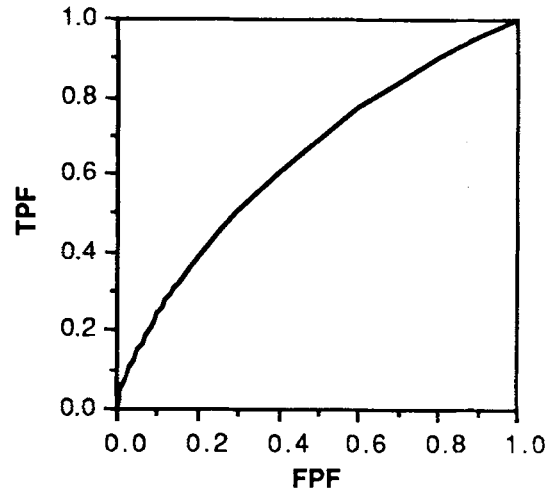


Fig 5. An ROC curve in which $A(z)$ is 0.645 with SD = 0.052.

Figure 5 shows an ROC curve in which $A(z)$ is 0.645 with SD = 0.052.

Experiment 3. The training set was 12 images consisting of 20 multiple nodules and 40 false nodules detected from the preliminary evaluation. The test set was 22 images consisting of 36 true nodules and 117 false nodules. (Some images were used in both sets, however, cases are not mixed in both sets). The number of nodes on the hidden layer was 200, and the number of output nodes was two.

Figure 6 shows an ROC curve in which $A(z)$ is 0.782 with SD = 0.044.

From the above data, it can be seen that different patterns of the neural network (the number of nodes in the hidden layer and in the output layer) do not affect the ROC area. It is interesting to see an increase in the ROC area with the use of some of the false-positive detections from the test images in the training set. This particular result indicates that the neural net would perform much better when more background information about the test images is provided.

DISCUSSION

Substantial work in the field of computer-aided diagnosis has been done by a group of researchers led by K. Doi^{13,14} in pulmonary nodule detection,^{9,10} interstitial lung diseases, analysis of heart size, detection of clustered microcalcification and mammographic masses, analysis of stenotic lesions, etc. Giger has presented two effective lung nodule detection meth-

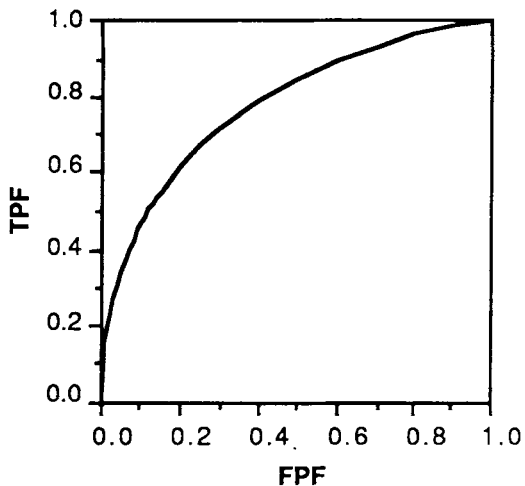


Fig 6. An ROC curve in which $A(z)$ is 0.782 with $SD = 0.044$.

ods: the evaluation of circularity with incremental thresholding and the evaluation of circularity using a morphological "open" operation. The results indicated that these methods achieved a true-positive detection rate of approximately 70% with an average of three to four false-positive detections per chest image. In their experiment, an image database consisting of 60 chest radiographs was used. Thirty chest images were normal and the remaining 30 radiographs contained nodules. Using a VAX-11/750 computer (Digital Equipment Corp, Maynard, CA), the process times for incremental thresholding and morphological operation methods were approximately 3 to 4 minutes and 1 hour, respectively.

Results of another independent research project in computer search of chest radiographs for lung nodules was presented by W. Lampeter and J. Wandtke.¹⁵ They manually masked the nonlung regions (ie, from the chest wall border to the sides and top of the radiograph, the regions of the diaphragm, mediastinum, and heart shadow). An image of the lung area was processed by a circle finder approach based on Hough transform^{16,19} and edge enhancement by a spline filter. Lampeter and Wandtke also used a "nodule expert" algorithm to classify suspected nodules based on a linear discriminant function. The experiment trained the program with 37 radiographs and can detect 92% true-positives of nodules using the same set of 37 radiographs. This program takes 30 minutes with a VAX 11/780.

There are several differences in the image processing algorithms used in our work and those previously reported. These are the use of a sphere profile matching algorithm that looks for the maximal fit by comparing the suspect area with several potential sphere profiles. Our total computer program is based on fast or semifast (due to memory swapping) algorithms and completes its task in approximately 35 seconds, substantially faster than prior programs. The neural network classifier was successful in getting the data to converge.

In experiments 1 and 2, the performance indices $A(z)$ of ROC curve are $\approx 64\%$ by using the neural network. Experiment 3 shows that the detection is greatly improved ($A[z] = 78\%$) when both training and testing use separate sets of image blocks, however, they share some images (ie, some of the image blocks in training and testing sets were selected from same chest images). The improvement performance in experiment 3 may result from two reasons (1) the correlation of both the training and the test image blocks from the same images in experiment 3 and (2) training image blocks were selected from only four chest images in experiments 1 and 2; thus, not many varieties of background information were learned by the neural network. We do not know which is the dominate factor, further evaluation using a larger database is planned.

The work reported here used image processing techniques as preliminary scanning methods to define suspected nodule areas. The final nodule classification was analyzed using back-propagation neural network. The neural network technique may offer advantages when compared with the image processing techniques alone. This is because the conventional image processing techniques result in several false-positive detections for each true-positive detection. We believe that some of the false-positive detections can be eliminated by the neural network. Further development of the algorithm and expansion of the data base are continuing.

ACKNOWLEDGMENT

The authors would like to thank Drs. Doi and Giger for their inspiration in the image processing aspect, fruitful comments from Dr. Nishikawa, and ROC programs from Dr. Metz. They are with Radiology Department at the University of Chicago.

REFERENCES

1. Horii SC, Mun SK, Levine BA, et al: PACS clinical experience at Georgetown University. *Comp Med Img and Graph* 15:183-190, 1990
2. Huang HK, Kangaroo H, Cho PS, et al: Planning a total digital radiology department. *AJR Am J Roentgenol* 54:635-639, 1990
3. Schmiedl UP, Rowberg AH: Literature Review: Picture archiving and communication systems. *J Digit Imaging* 3:238-245, 1990
4. Stitik FP, Tockman MS, Khouri NF: Chest radiology, in Miller AB (ed): *Screening for Cancer*. New York, NY, Academic, 1985, pp 163-191
5. Heelan RT, Flechinger BJ, Melamed MR, et al: Non-small cell lung cancer: Results of the New York screening program. *Radiology* 151:289-293, 1984
6. Montain CF: Value of the new TNM staging system for lung cancer. *Fifth World Conference on Lung Cancer*. *CHEST* 96:47s-49s, 1989 (suppl)
7. Lo SC, Taira RK, Mankovich NJ, et al: Performance characteristics of a laser scanner/printer system for radiological imaging. *J Comp Radio* 10:227-237, 1986
8. Shaw C-G, Herron JM, Gur D: Pixel average versus digitization using larger apertures—A comparison of the spatial resolution properties. *SPIE Proc Med Img VI* 1651:128-131, 1992
9. Giger ML, Doi K, MacMahon H: Image feature analysis and computer-aided diagnosis in digital radiography. 3. Automated detection of nodules in peripheral lung field. *Med Phys*. 15:158-166, 1988
10. Giger ML, Ahn N, Doi K, et al: Computerized detection of pulmonary nodules in digital chest images: Use of morphological filters in reducing false-positive detections. *Med Phys* 17:861-865, 1990
11. Rumelhart DE, Hinton GE, Williams RJ: Learning internal representations by error propagation, in Rumelhart PE, McClelland JL (eds): *Parallel Distributed Processing: Explorations in the Microstructure of Cognition*, vol 1: Foundation. Cambridge, MA, Massachusetts Institute of Technology, 1986
12. Swets JA, Pickett RM: *Evaluation of Diagnostic Systems*, New York, NY, Academic, 1982
13. Doi K: Feasibility of computer-aided diagnosis in digital radiography. *Jap J Radio Tech* 45:653-663, 1989
14. Doi K, Giger ML, MacMahon H, et al: Clinical radiology and computer-aided diagnosis: Potential partner in medical diagnosis? *Radiological Society of North America Scientific Exhibit*, Space 129, Chicago, IL, December 1990
15. Lampeter WA, Wandtke JC: Computerized search of chest radiographs for nodules. *Invest Radiol* 21:384-390, 1986
16. Hough PVC: A method and means for recognizing complex patterns. *US Patent* 3,069,654
17. Illingworth J, Kitter J: A survey of the Hough transform. *Computer, Vision, Graphics, Image Proc*, 44:87-116, 1988